JOURNAL OF SOLID STATE CHEMISTRY 114, 346–358 (1995)

The Crystal Chemistry and Role of Metal–Metal Bonding in the Monochalcogenides TiS, VS, TiSe, and VSe and Their Solid Solutions

L. Henderson Lewis[1] and J. B. Goodenough

Center for Materials Science and Engineering, The University of Texas at Austin, Austin, Texas 78712

Received February 8, 1994; in revised form April 20, 1994; accepted April 21, 1994

The influence of metal–metal bonding on the physical properties of the titanium and vanadium monosulfides, monoselenides, and their solid solutions is explored. Compounds were synthesized at 800°C and characterized by room-temperature X-ray diffraction, chemical analysis, density, differential thermal analysis (DTA), magnetic susceptibility, and electrical resistance. All compounds formed one of three closely related crystal structures: hexagonal $B8_1$, orthorhombic $B31$, or a rhombohedral $9R$ polytype. In all these structures, partially occupied orbitals of $3d$ parentage form narrow bands as a result of metal–metal interactions; all compounds were metallic and Pauli paramagnetic except nominal VSe, which exhibits an antiferromagnetic Néel temperature $T_N \cong 240$ K and becomes semiconductive below 50 K. Evidence of anion vacancies was found for all samples; compounds formed from larger selenium atoms also incorporate interstitial metals into trigonal bipyramidal sites, stabilizing the hexagonal $B8_1$ structure and avoiding distortions to the ideal ("unstuffed") $B31$ or $9R$ structures.

1. INTRODUCTION

The influence of metal–metal bonding on the physical properties of Ti and V compounds is of interest because the partially occupied $3d$ orbitals form narrow bands. Depending on the strength of the metal–metal interactions, the $3d$ electrons may be localized, itinerant, or trapped in metal-atom clusters (1). TiO and VO appear to crystallize in the cubic rocksalt structure, for example, but both the cation and the anion sublattices contain about 16% vacancies; in these oxides, the vacancies reduce the lattice parameter and therefore increase the metal–metal bonding across shared octahedral-site edges. Ordering of the vacancies occurs in superconductive TiO; the vacancies remain disordered in the semimetal VO.

The nominal monochalcogenides TiX and VX, X = S or Se, crystallize either in the hexagonal $B8_1$ structure of NiAs or a hexagonal $9R$ polytype or the orthorhombic $B31$ structure of MnP. In this paper we explore the influence of metal–metal bonding on the chemistry and structure of four nominal monochalcogenide systems, TiS–VS, TiSe–VSe, TiS–TiSe, and VS–VSe.

2. CRYSTAL STRUCTURES

The ideal $B8_1$ structure consists of a close-packed hexagonal anion array with cations in the octahedral sites. In this structure, each anion is at the center of a trigonal-prismatic site of a primitive hexagonal cation array; the cations share octahedral-site faces along the hexagonal c-axis and share octahedral-site edges within a basal plane. The tetrahedral sites form face-shared pairs to make a single trigonal bipyramidal interstitial site. The bipyramidal sites share common faces with the occupied octahedral sites.

Nonstoichiometry is commonly encountered in the monochalcogenides. Cation vacancies tend to order within alternate octahedral-site basal planes of the hexagonal $B8_1$ structure in a sequence of discrete $M_{1-x}X$ compounds over the compositional range $0 \leq x \leq 0.5$ (2). However, as in Ti_8S_9, cation vacancies may also induce formation of a 9R polytype in which the stacking of close-packed anion planes is $(chh)_3$, where c denotes cubic and h denotes hexagonal stacking; the cations occupy octahedral sites in this phase also. Two types of metal-rich compounds are found: $M_{1+x}X_{1-y}$ compounds ($0 < x \leq 1$) contain cation interstitials that occupy randomly the bipyramidal sites, and MX_{1-y} compounds contain a small ($y < 0.1$) concentrations of anion vacancies. The metal-rich compounds have an atom-deficient hexagonal close-packed anion array of the $B8_1$ structure.

A stoichiometric or metal-poor phase may have the $B31$ structure, which is derived from the $B8_1$ phase by cooperative atomic displacements that create zigzag metal-atom chains and anion (or metalloid) chains each running parallel to the orthorhombic a-axis. This geometric relationship allows for two possible driving forces for the transition from $B8_1$ to $B31$ symmetry: optimization of

[1] To whom correspondence is to be addressed at present address: Materials Science Division, Brookhaven National Laboratory, Upton, New York 11973.

0022-4596/95 $6.00

metal–metal bonding associated with narrow, partially filled $3d$ bands, and/or the optimization of metalloid–metalloid bonding associated with partially filled metalloid p bands. Franzen *et al.* (3) have provided a crystallographic criterion for distinguishing which distortion mechanism is dominant: in space group *Pmcn* for the *B*31 phase, an axial ratio $c/b > 0.943$ signals metal–metal bonding and a $c/b < 0.943$ indicates metalloid–metalloid bonding; a $c/b = 0.943$ is the "ideal" ratio for hexagonal close packing with $b = (\sqrt{3})a$. The resultant concentration of electrons in the shorter metal–metal bonds and/or holes in the metalloid–metalloid bonds is sometimes referred to as a charge-density wave (CDW) state.

The titanium and vanadium monochalcogenides have partially filled $3d$ orbitals with the Fermi energy E_F above the top of the chalcogenide valence bands. The cubic component of the crystalline field at the octahedrally coordinated cations splits the fivefold orbital degeneracy of the metal-atom $3d$ states into three degenerate t_2 orbitals and two degenerate e orbitals of higher energy. In an hexagonal lattice, a trigonal component of the crystalline field further splits the threefold degeneracy of the t_2 orbitals into two degenerate e_π orbitals and a nondegenerate a_1 orbital. The a_1 orbitals are directed along the hexagonal c-axis; the a_1 orbitals of nearest cation neighbors along the c-axis overlap across a shared octahedral-site face. The two e_π orbitals are each extended toward three of the six cation near neighbors in a basal plane making 120° M–M bond axes; they are rotated with respect to each other by 60°. This geometry allows two e_π electrons per metal atom to bond to all six near neighbors in the basal plane via half-filled e_π bands. The relative stabilities of the a_1 and e_π orbitals depend critically on the axial ratio c/a of the crystal (4). In the *B*31 structure, a 60° angle between the metal–metal bonds of a metal-atom chain allows both e_π orbitals to participate in metal–metal bonding, and the change in translational symmetry from that of the hexagonal $B8_1$ structure opens up an energy gap in the e_π bands at the half-band position.

3. PREVIOUS WORK

The first large-scale systematic studies on the transition-metal chalcogen/pnicogen systems were performed in 1937 by Biltz *et al.* (5). This interest was sustained until the late 1970s, and a large number of thorough review articles exist that summarize the results generated during that period (6–13). More recently, a number of researchers have performed band-structure calculations of various types in an attempt to elucidate some of the physical and chemical properties found in these systems (14–20). In this section we summarize the experimental information available in the literature on the compounds TiS, VS, TiSe, and VSe and on the system $(V_{1-x}Ti_x)S$, as well as the pertinent results from the band-structure calculations. In general, all of the compounds studied have homogeneity ranges that are strongly dependent upon preparation temperature. All compounds are reported to be metallic and, except for VSe, to exhibit Pauli paramagnetism.

Stoichiometric TiS does not appear to exist; the metal-rich TiS_{1-x} ($x \cong 0.05$) phases have the $B8_1$ structure with an unusually high $c/a \approx 1.92$ axial ratio and the sulfur-rich $Ti_{1-x}S$ phases form the $9R$-polytype structure with metal-atom vacancies (21). X-ray photoelectron spectroscopy has confirmed that the S $3p$ valence bands lie below E_F, which is located within the partially filled Ti $3d$ bands (22).

Stoichiometric VS is reported (23) to have the theoretical density and orthorhombic *B*31 structure at room temperature. A range of nonstoichiometry is stable on either side of the stoichiometric compositions. The existence of three different hexagonal $B8_1$ type phases is reported in the range $V_{0.89}S$ to $V_{0.98}S$ (9). It is stated that metal-rich VS_{1-x} samples contain sulfur vacancies; metal-poor VS_{1+x} samples contain vanadium vacancies (24). At room temperature, the *B*31 phase is stable for $0.85 \leq S/V < 1.06$ (10); the structure changes from *B*31 to $B8_1$ at a S/V ratio of 1.06 (23, 25). A second-order *B*31–$B8_1$ transition occurs at $T_t = 350$°C in $V_{0.95}S$; the transition temperature increases to 630°C as the stoichiometric composition VS is approached (26–28). X-ray photoelectron spectroscopy (28) indicates that the filled valence bands lie discretely below E_F, which lies in the partially filled V $3d$ bands of a_1 and e_π parentage. However, the V–S bonding via the σ-bonding V e, s, and p orbitals is reported to be so strong that there is little charge transfer from V to S (22, 29); the valence bands are described with a band model rather than with a crystal field model, i.e., a covalent rather than an ionic model. Magnetic-susceptibility measurements show an enhanced Pauli paramagnetism with the presence of some localized spins, which we associate with anion vacancies (26–28, 30–32).

TiSe does not exist in a stoichiometry form; it disproportionates into an anion-deficient *B*31 phase reported to be $TiSe_{0.95}$ and an hexagonal phase initially thought to be the cation-deficient $B8_1$ phase $Ti_{0.95}Se$ (33) but later contended to be a Ti_8Se_9 phase with an ordering of the Ti vacancies that serves to minimize electrostatic repulsion (34). In addition, a rhombohedral form of TiSe with unknown composition was obtained by Hahn and Ness (35); it is shown in this work to be isostructural with the $9R$ polytype of Ti_8S_9 identified by Hahn and Harder (36). An anomaly at 630°C in the signal obtained from differential thermal analysis (DTA) performed on the *B*31 form of $TiSe_{0.95}$ was observed by Hirota *et al.* (37), who were unable to identify the cause of the anomaly because the sample reacted with the silica tube in which it was sealed.

VSe has the hexagonal $B8_1$ structure at all temperatures

studied (11, 26, 38–40). Of the four end-member monochalcogenides investigated in this work, only nominal VSe has an axial ratio $c/a = 1.62$ close to the ideal ratio 1.633 for hexagonal close packing. A diffusion-controlled transition in the interval $550\ \text{K} < T < 650\ \text{K}$ was noted by Carpay (11) in samples slow-cooled to 300°C; he speculated that metal–metal bonding in VSe is enhanced by the introduction of vacancies on both the cation and anion sublattices. Resistance measurements indicate that VSe exhibits poor metallic behavior (41), and the magnetic susceptibility data indicated a strongly enhanced Pauli paramagnetism with apparent Curie–Weiss behavior, but with a Weiss constant of −2570 K and a spin-only effective moment of $3.2\ \mu_B$ indicative of narrow-band magnetism (11). Possible Néel temperatures of $T_N \cong 300$ K (39), 163 K (26), and 100 K (11) have been reported.

The effects of a changing Ti : V ratio on the structure of the compounds in the $(V_{1-x}Ti_x)S$ system have been studied by Leebrick (42), Franzen *et al.* (24) and by the present authors (43). Samples synthesized by arc-melting followed by high-temperature (1400°C ≤ T ≤ 1600°C) annealing (42, 24) showed an essentially smooth $B31$–$B8_1$ transformation with increasing x at the composition $(V_{0.65}Ti_{0.35})S$; it was suggested (24) that the crystallographic change occurs at a critical electronic concentration of 0.270 $e^-/\text{Å}^3$. Samples prepared by low-temperature ($T \cong 800$°C) annealing gave a sharp transformation from the $B31$ to the $B8_1$ structure around the composition $(V_{0.65}Ti_{0.35})S$ and a deviation from Végard's law in the interval $0.40 \le x \le 0.60$ where the $B31$ phase appears to be suppressed (43). All samples were found to be Pauli paramagnetic, and there is no special change in the nature of the magnetic signal at the $B31/B8_1$ compositional borderline.

All band calculations (14–20) show strong σ-bond metal–metalloid interactions that split antibonding states from bonding states. In the $B8_1$ structure, the parentage of the empty antibonding states of the $(V_{1-x}Ti_x)S_{1\pm y}$ system have primarily cation e, s and p character; the filled valence bands have primarily S $3p$ character. The Fermi energy E_F lies within partially filled, narrow bands of cation a_1 and/or e_π parentage that are essentially nonbonding with respect to the metal–sulfur interactions. The dispersion in these narrow bands appears to be primarily due to metal–metal interactions. However, there is disagreement about the relative energies of the bands of a_1 and e_π parentage, which depend sensitively on the axial ratio c/a. We will argue that this issue is especially important for understanding the variation with x of the c/a ratio in the nominal system $(V_{1-x}Ti_x)S_{1\pm y}$.

4. SYNTHESIS AND EXPERIMENTAL PROCEDURES

Samples were synthesized from stoichiometric mixtures of the elements; the purity of the powdered metals was 99.5–99.8%, and the purity of the lump-form metalloids was in the range 99.999–99.9995%. Required quantities of the elements were ground, pelletized, and placed in silica tubes under an argon atmosphere in a glovebox. The charged silica tubes were then evacuated to a pressure $P < 1 \times 10^{-5}$ Torr and sealed. Samples were heated at 100°C/day to 800°C; they were slow-cooled after being held for 5 days at 800°C. The sealed tubes were either placed upright or inclined at an angle during the initial heating cycle to ensure that the low-melting chalcogens did not flow to the opposite end of the tube and condense. Regrinding the product under argon and refiring at 800°C for 5 to 7 days was always repeated a second time in order to obtain samples that were single-phase under powder X-ray diffraction. In some instances, the regrinding, resealing, and reannealing procedure was repeated up to five times. No reaction with the silica tube was observed except for those samples that contained both titanium and selenium together.

Room-temperature lattice parameters were obtained from a least-squares-fitting routine (44) of powder X-ray diffraction patterns taken with monochromatic CuK_α radiation in the range $10° \le 2\theta \le 60°$. DTA measurements were performed on nominal TiSe sealed in evacuated ($P < 1 \times 10^{-5}$ Torr), thin-walled silica capillary tubes to observe possible phase transformations. After thermal cycling, a silvery-gray coating was noticed on the inside of the capillary tube.

The density of each sample was measured with a fully automated Micromeritics, Inc. AccuPyc 1330 helium pycnometer. A specially designed 0.1-cm^3 sample cup was used to measure the volumes/densities of small amounts of the dry and finely powdered samples. After an automated purge cycle, each sample was subjected to a run that involved five separate volume determinations. Each sample was measured at least two times to monitor reproducibility. The accuracy of the pycnometer is approximately ±0.0002 g/cm^3, but the uncertainty used in the calculation of atomic occupancy is taken to be the standard deviation of three or more separate measurements. Density measurements may be complicated by two problems. First, anion rejection from the lattice can result in amorphous chalcogenide at the surface and grain boundaries that are not detected by X-ray diffraction but do increase the total volume measured, thereby lowering the apparent density. Second, the particles may contain voids, thereby again lowering the apparent density. Therefore density measurements were made on finely powdered samples; this method of measurement also avoids problems with particle agglomeration. Lattice occupancies were calculated for all samples with the method of van Gool (45). The error in the calculated atomic occupancies is determined with standard error analysis (46).

Chemical analyses were done on each system with en-

ergy-dispersive X-ray spectroscopy (EDS). Polished samples of titanium metal and vanadium metal, as well as selenium metal shot and powdered In_2S_3, were used as standards. The K_α peaks of Ti, V, and S and the L_α peak of Se were examined in each case; there is no peak overlap at the energies involved. A difference between the composition on the surface of the sintered pellets and that of the interior of the pellets was always noted. For this reason, the compositional analyses were done on finely powdered samples from the interior of the pellets that were not allowed to sit in air for more than five min. A small amount of fluffy, poorly crystallized material was detected by SEM in all samples. It was thought that this material might be amorphous, and thus the compositional analyses were performed only on euhedral crystallites. No charging was noticed on any sample, and each sample appeared to be undamaged after the analyses were performed. Five separate analyses were performed on each sample to obtain a statistically averaged composition.

Two samples, $(Ti_{0.5}V_{0.5})S$ and $(Ti_{0.6}V_{0.4})S$, were arc-melted in water-cooled copper crucibles in an attempt to reproduce the results of Franzen *et al.* (24). Transmission electron microscopy was performed on two samples, $V(S_{0.5}Se_{0.5})$ and arc-melted $(Ti_{0.5}V_{0.5})S$, in an attempt to identify the composition and clarify some of the details of the very fine-scale microstructure.

Low-temperature magnetic-susceptibility measurements were made from 5 to 320 K in an applied field of 10 kOe with a SQUID magnetometer. The four-probe method was used to measure electrical resistance from room temperature down to 10 K on pressed, sintered cylindrical samples with an average facial surface area of 20 mm^2 and an average thickness of 1.0 mm. The accuracy of the resistance determinations is on the order of 1%.

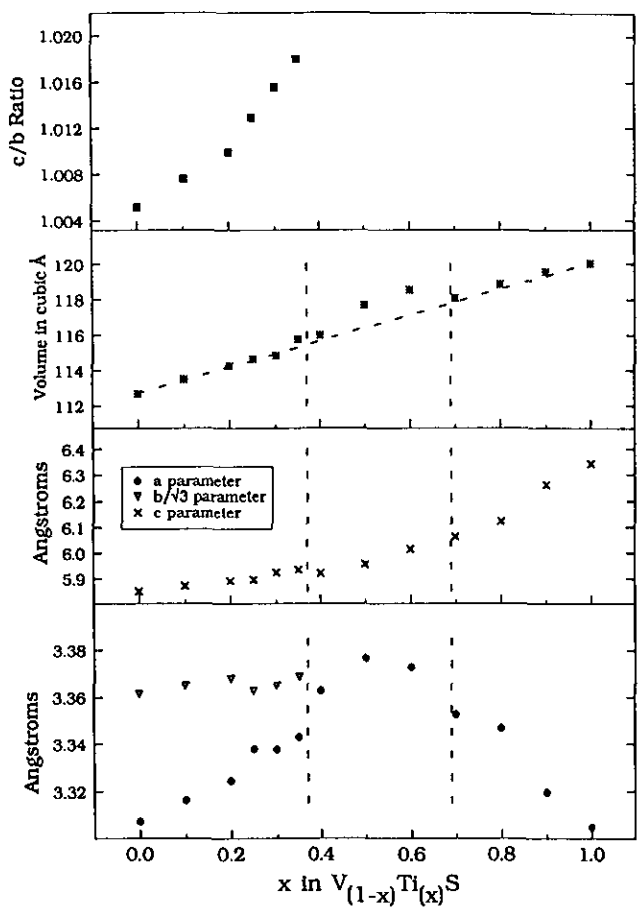

FIG. 1. Lattice parameters, unit-cell volumes, and c/b ratios for the nominal $(V_{1-x}Ti_x)S$ system.

5. EXPERIMENTAL RESULTS

5.1. The $(V_{1-x}Ti_x)S$ System

By visual inspection, samples in the $(V_{1-x}Ti_x)S$ system did not react with the quartz tubes and all the sulfur was incorporated into the compounds. Figure 1 shows the evolution with x of the room-temperature lattice parameters, the orthorhombic c/b ratio, and the volume (43). A $c/b > 0.943$ in the $B31$ phase signals that the distortion is driven by metal–metal bonding in the basal planes. The lattice parameters of the end-member compositions TiS and VS agree well with published values (21, 47). However, comparison of the lattice-parameter data for arc-melted samples (24, 43) with those of Fig. 1 shows a significant discrepancy in the compositional range $0.40 \leq x \leq 0.65$; the arc-melted samples had the orthorhombic $B31$ structure at room temperature whereas those prepared at 800°C (Fig. 1) are hexagonal. Nevertheless, both sets of data show a definite deviation from Végard's law to a larger volume in this range and the average basal-plane parameter $\langle a \rangle = \frac{1}{2}[(b/\sqrt{3}) + a]$ shows a maximum near $x \cong 0.5$ for each set.

All the samples prepared at 800°C have a sulfur/metal ratio less than unity ($S/M < 1$), and the measured densities correspond, with the exception of $x = 0.30$, to a filled metal-atom array and sulfur vacancies (see Fig. 2 and Table 1). For the $x = 0.30$ sample, the density measurement indicates vacancies on both cation and anion sublattices. Franzen *et al.* (24) reported a $S/M > 1$ in the interval $0.40 \leq x \leq 0.65$ with a density requiring the improbable introduction of interstitial sulfur atoms. Although their density measurements are probably not reliable, it appears that the arc-melted samples have a higher S/M ratio than those prepared at 800°C.

Samples $(V_{0.5}Ti_{0.5})S$ and $(V_{0.4}Ti_{0.6})S$ were arc-melted in an attempt to reproduce the results of Franzen *et al.* (24). During the procedure it was observed that the samples did cross over to the liquid state, and X-ray diffraction proved that after melting both samples transformed upon cooling from the $B8_1$ phase to the $B31$ phase. Neverthe-

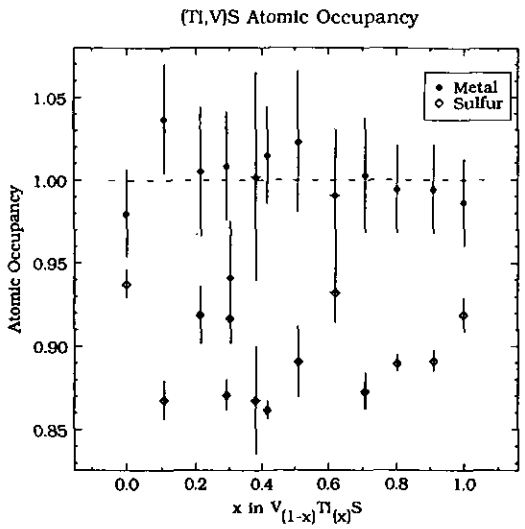

FIG. 2. Atomic occupancies of the $(V_{1-x}Ti_x)S$ system.

less, the c-parameters, the unit-cell volumes and the c/b ratios of the arc-melted samples all extrapolate smoothly from the non-arc-melted values, which indicates that any overall compositional change induced by the arc melting is small. A small amount of unidentified second phase was found to be present in both arc-melted samples; it was subsequently examined in the $(Ti_{0.5}V_{0.5})S$ sample with TEM X-ray elemental analysis and electron diffraction and found to be approximately cubic with a lattice parameter $a \cong 6$ Å. There is no evidence of sulfur in this phase, and the titanium : vanadium ratio was around 3 : 1; this phase is most probably an oxide or a nitride.

With the exception of samples $(V_{0.6}Ti_{0.4})S$ and $(V_{0.5}Ti_{0.5})S$, which have resistances one order of magnitude larger than those of the other samples, the resistances

TABLE 1
The $V_{1-x}Ti_xS$ System

Nominal composition	S : M ratio	Density (g/cm³)	Calculated stoichiometry
VS	0.96 ± 0.014	4.71 ± 0.006	$V_{0.98}S_{0.94}$
$V_{0.9}Ti_{0.1}S$	0.84 ± 0.010	4.70 ± 0.007	$(V_{0.89}Ti_{0.11})_{1.04}S_{0.87}$
$V_{0.8}Ti_{0.2}S$	0.91 ± 0.021	4.65 ± 0.009	$(V_{0.79}Ti_{0.22})_{1.01}S_{0.92}$
$V_{0.75}Ti_{0.25}S$	0.86 ± 0.014	4.54 ± 0.02	$(V_{0.71}Ti_{0.29})_{1.01}S_{0.87}$
$V_{0.7}Ti_{0.3}S$	0.97 ± 0.022	4.40 ± 0.008	$(V_{0.70}Ti_{0.30})_{0.94}S_{0.92}$
$V_{0.65}Ti_{0.35}S$	0.87 ± 0.034	4.46 ± 0.003	$(V_{0.62}Ti_{0.38})_{1.00}S_{0.87}$
$V_{0.6}Ti_{0.4}S$	0.86 ± 0.009	4.48 ± 0.008	$(V_{0.58}Ti_{0.42})_{1.02}S_{0.87}$
$V_{0.5}Ti_{0.5}S$	0.87 ± 0.019	4.47 ± 0.006	$(V_{0.49}Ti_{0.51})_{1.02}S_{0.89}$
$V_{0.4}Ti_{0.6}S$	0.94 ± 0.024	4.40 ± 0.006	$(V_{0.38}Ti_{0.62})_{0.99}S_{0.93}$
$V_{0.3}Ti_{0.7}S$	0.87 ± 0.016	4.33 ± 0.003	$(V_{0.29}Ti_{0.71})_{1.00}S_{0.87}$
$V_{0.2}Ti_{0.8}S$	0.90 ± 0.009	4.29 ± 0.004	$(V_{0.20}Ti_{0.80})_{0.99}S_{0.89}$
$V_{0.1}Ti_{0.9}S$	0.90 ± 0.008	4.25 ± 0.011	$(V_{0.09}Ti_{0.91})_{0.99}S_{0.89}$
TiS	0.93 ± 0.007	4.25 ± 0.012	$Ti_{0.99}S_{0.92}$

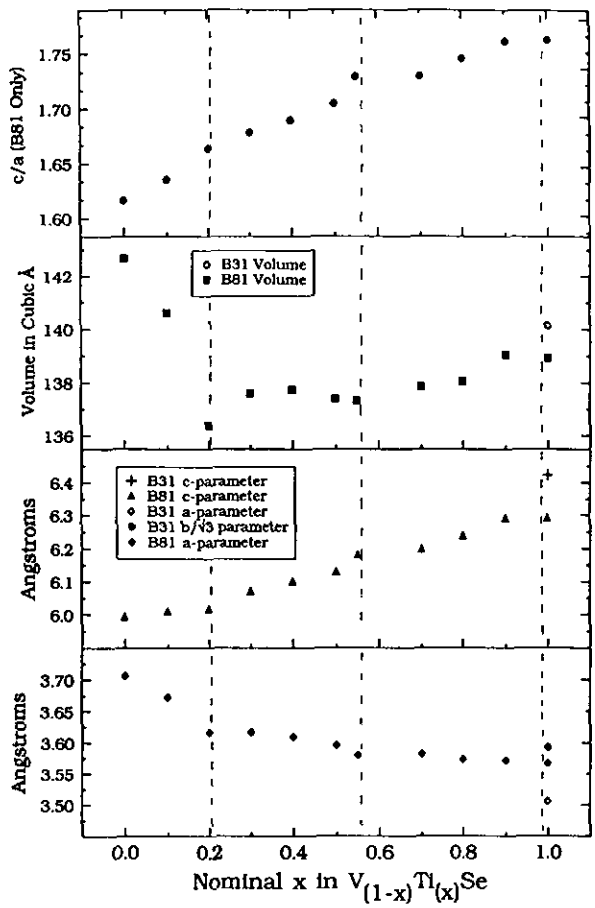

FIG. 3. Lattice parameters, unit-cell volumes, and c/a ratios for the nominal $(V_{1-x}Ti_x)Se$ system.

of all samples in the $(V_{1-x}Ti_x)S$ system are small, nearly temperature-independent, and reversible on cycling between 4 and 300 K.

As reported (26–28, 30–32) for the end-member VS, all the samples exhibited an enhanced Pauli paramagnetism with evidence at low temperatures of localized spins associated with the sulfur vacancies.

The $B31$ samples ($x < 0.40$) showed a hysteretic DTA anomaly at a transition temperature $T_t \cong 580$°C that varied from 520°C to 620°C with a varying S/M ratio. We assume that this marks the $B31$–$B8_1$ transition in this system.

5.2. *The $(V_{1-x}Ti_x)Se$ System*

During synthesis, a moderate coating of the silica tube was noticed after the first anneal, and light, grayish coatings were noticed upon subsequent annealings. The lattice-parameter data of Fig. 3 were obtained on samples that had been annealed at least twice. From Figs. 3 and 4 and Table 2, four distinct compositional regions are apparent: (a) $0 \leq x < 0.2$ is characterized by a decrease in the volume of the $B8_1$ phase with increasing x despite

TABLE 2
The $V_{1-x}Ti_xSe$ System

Nominal composition	Se : M ratio	Density (g/cm^3)	Calculated stoichiometry
VSe	0.76 ± 0.015	5.75 ± 0.003	$V_{1.12}Se_{0.84}$
$V_{0.9}Ti_{0.1}Se$	0.67 ± 0.015	5.73 ± 0.006	$(V_{0.88}Ti_{0.12})_{1.16}Se_{0.79}$
$V_{0.8}Ti_{0.2}Se$	0.86 ± 0.004	5.88 ± 0.001	$(V_{0.79}Ti_{0.21})_{1.05}Se_{0.83}$
$V_{0.7}Ti_{0.3}Se$	0.86 ± 0.019	5.89 ± 0.006	$(V_{0.65}Ti_{0.35})_{1.06}Se_{0.83}$
$V_{0.6}Ti_{0.4}Se$	0.70 ± 0.013	5.88 ± 0.002	$(V_{0.663}Ti_{0.37})_{1.16}Se_{0.81}$
$V_{0.5}Ti_{0.5}Se$	0.77 ± 0.012	5.89 ± 0.001	$(V_{0.46}Ti_{0.54})_{1.08}Se_{0.77}$
$V_{0.4}Ti_{0.6}Se$	0.78 ± 0.018	5.68 ± 0.003	Unknown phase
$V_{0.3}Ti_{0.7}Se$	0.79 ± 0.008	5.59 ± 0.001	Unknown phase
$V_{0.3}Ti_{0.7}Se_{1.05}$	0.65 ± 0.009	5.70 ± 0.005	$(V_{0.31}Ti_{0.69})_{1.18}Se_{0.77}$
$V_{0.2}Ti_{0.8}Se$	0.76 ± 0.060	5.75 ± 0.005	$(V_{0.18}Ti_{0.82})_{1.10}Se_{0.84}$
$V_{0.1}Ti_{0.9}Se$	0.80 ± 0.021	5.54 ± 0.004	Unknown phase
$V_{0.1}Ti_{0.9}Se$	0.74 ± 0.014	5.67 ± 0.001	$(V_{0.095}Ti_{0.91})_{1.11}Se_{0.82}$
$TiSe_{0.95}$ (B31)	0.86 ± 0.019	5.58 ± 0.005	$Ti_{1.02}Se_{0.87}$
$TiSe_{1.05}$	0.75 ± 0.021	5.74 ± 0.005	$Ti_{1.10}Se_{0.83}$

the larger size of Ti^{2+} relative to V^{2+}; (b) $0.2 \leq x \leq 0.6$ has a volume of the $B8_1$ phase that is nearly independent of composition and a relatively large density; (c) $0.6 < x < 1.0$ has the $B8_1$ phase only if the selenium/metal ratio is $Se/M \leq 0.76$ and the $B8_1$ volume increases with x; and (d) $x = 1.0$ disproportionates into a $B31$ phase with Se/Ti ≥ 0.86 and a $B8_1$ phase with Se/Ti ≤ 0.75.

From density measurements, all the samples with the $B8_1$ structure contain interstitial metal atoms (Fig. 4 and Table 2), whereas nominal $TiSe_{0.95}$ with the $B31$ structure does not; this difference is reflected in a smaller density for the $B31$ versus the $B8_1$ phase for $x = 1.0$. The lattice parameters of the end-member nominal compositions VSe, $TiSe_{0.95}$, and $TiSe_{1.05}$ agree with those reported in the literature (11, 33). The nominal $TiSe_{1.05}$ sample showed evidence of a small amount of second phase. Brunie and Chevreton (34) obtained a $B8_1$ single phase starting from $TiSe_{1.12}$ (Ti_8Se_9) that exhibited ordering of Ti vacancies in every other basal plane; the $B8_1$ phase obtained from nominal $TiSe_{1.05}$ in this study shows no superstructure lines and has Ti interstitials as opposed to Ti vacancies. On the other hand, a single crystal of the Brunie–Chevreton phase Ti_8Se_9 with the appropriate density was grown during the course of this work. Thus it appears that the hexagonal phase observed by Grønvold and Langmyhr (33) is to be distinguished from the ordered Ti_8Se_9 phase identified by Brunie and Chevreton (34). It should also be noted that the $B31$ phase has a significantly larger c-parameter as well as a lack of interstitial metal atoms as compared with the $B8_1$ phase. Finally, a $c/b > 0.943$ in the $B31$ phase indicates that the distortion is due to metal–metal interactions in accordance with the criterion of Franzen *et al.* (3).

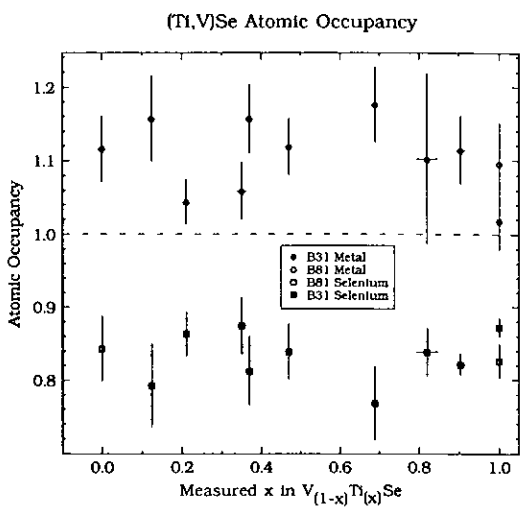

FIG. 4. Atomic occupancies of $(V_{1-x}Ti_x)Se$.

A DTA study of the $B31$ sample of TiSe was made in quartz with multiple thermal cycling between 100°C and 800°C. Hirota *et al.* (37) found a DTA anomaly near 630°C, but they were unable to confirm the transformation to the $B8_1$ phase with high-temperature X-ray diffraction because of reaction with their silica tube. The $B31$ sample of nominal $TiSe_{0.95}$ in Table 2 showed a broad exothermic peak with a minimum at 540°C on first heating; this peak was generally not observed on subsequent heatings at 20°C/min. Quenching of bulk $B31$ $TiSe_{0.95}$ from 625°C gave a room-temperature X-ray pattern that showed the presence of the $B8_1$ structure plus a small amount of a second phase. No reaction with the tube was visible in this experiment other than the appearance of a slight shadow on the circumference of the tube nearest the sample after opening the tube under argon. Since a displacive $B31$–$B8_1$ transition should have been reversible, we are forced to conclude that between 540°C and 625°C a diffusional process and some loss of material has accompanied or followed the $B31$–$B8_1$ transition at 540°C and that this diffusional process stabilizes the $B8_1$ phase. Such a process could be the migration of metal atoms to the interstitial positions accompanying preferential loss of selenium. The presence of interstitial metal atoms would introduce competitive metal–metal bonding and thereby inhibit the cooperative bonding transformation to the $B31$ structure. On cooling from 800°C, an exothermic peak occurred at 630°C that does not appear to be associated with the irreversible $B31$–$B8_1$ transition that appears to occur at 540°C. This peak at 630°C is found on subsequent cooling cycles along with an additional peak that appears at 575°C and becomes larger by the fifth cooling run (these peaks were not detected upon heating). After the fifth cycle, the resultant X-ray diffraction pattern indicates that the sample had largely transformed to a $B8_1$ phase, but retained a $B31$ component. Thus some reversibility of the $B8_1$–$B31$ tran-

sition is seen on cooling at 20°C/min, which reinforces the speculation that the reversible displacive transition is made irreversible by a migration of metal atoms in the hexagonal phase to interstitial sites that is stabilized by a diffusion-controlled loss of selenium. The transitions at 630°C and 575°C appear to be associated with the $B8_1$ phase; they could be order–disorder transitions that involve cation transfer to/from interstitial sites. Roberts showed a $B8_1$–$B8_1$ reversible transition in MnBi at 340°C to 360°C in which 10% of the Mn atoms migrated to the interstitial bipyramidal sites above 360°C. A similar reversible migration may occur in the hexagonal $B8_1$ form of TiSe at 630°C, the transition identified by Hirota *et al.* (37). The appearance of metal interstitials in the selenides, but not in the sulfides, is compatible with the larger size of the Se atoms and hence the larger metal–metal distances across a shared face of the octahedral and interstitial bipyramidal sites.

Previous workers that have studied VS_{1+x} have emphasized that the $B31$ phase occurs for valence–electron concentrations greater than a critical value (23); in TiSe the $B31$ phase occurs for a valence–electron concentration less than a critical value. Thus the criterion is not very meaningful.

The susceptibility χ versus temperature measurements for the $(V_{1-x}Ti_x)Se$ system show evidence for an itinerant-electron Néel temperature between 200 and 300 K in the $x = 0$ and 0.1 samples; the paramagnetic susceptibility at higher temperatures is nearly temperature-independent and decreases essentially linearly with x. At temperatures below 40 K, the marked increase in χ with decreasing temperature found in all $(V_{1-x}Ti_x)Se$ samples, excluding both forms of TiSe, signals the presence of localized spins that are not coupled to any magnetic ordering. The persistence of intrinsic localized spins at low temperatures in all anion-deficient samples indicates that the anion vacancies are acting as odd-electron traps.

Samples in the $(V_{1-x}Ti_x)Se$ system, aside from VSe, exhibit a small, semimetallic resistance that lies in the range 2×10^{-3} to 7×10^{-3} Ω and has a relatively small temperature dependence. The resistance of VSe increased sharply below 25 K and showed a slight thermal hysteresis in the range 100 K $< T <$ 200 K where the magnetic susceptibility showed anomalies suggestive of a Néel temperature. It would appear that antiferromagnetic order opens a gap at the Fermi energy below T_N.

5.3. *The $Ti(Si_{1-x}Se_x)$ System*

During the preparation of the $Ti(S_{1-x}Se_x)$ samples, material was always rejected from the bulk to coat the sides of the silica tube for those samples with compositions in the range $0.05 < x \leq 0.9$. SEM EDS analysis of this coating

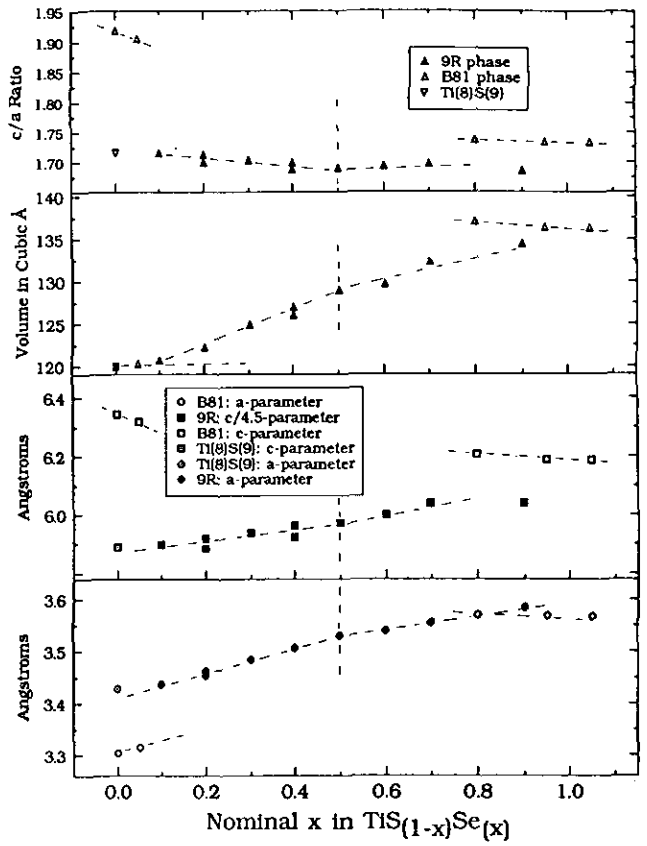

FIG. 5. *Lattice parameters, unit-cell volumes, and c/a ratios for the* nominal $Ti(S_{1-x}Se_x)$ system.

on several samples revealed that it consisted entirely of titanium and silicon; no sulfur or selenium was detected in the EDS spectrum. When all samples were examined with X-ray diffraction, it was discovered that $Ti(S_{1-x}Se_x)$ samples with compositions in the interval $0.1 \leq x \leq 0.7$ and with $x = 0.9$ crystallized with the rhombohedral $9R$ polytype structure isostructural with Ti_8S_9. Figure 5 displays the lattice parameters, unit-cell volumes, and c/a ratios for the $Ti(S_{1-x}Se_x)$ samples as functions of composition. The $9R$ c lattice parameters have been divided by 4.5 so that the hexagonal $B8_1$ structure and the rhombohedral $9R$ structure can be directly compared to one another. The $B31$ sample $TiSe_{0.95}$ is not included in this figure, but the Ti_8S_9 lattice parameters of Bartram (21) are shown. There is a sharp discontinuity in the a and c lattice parameters as the structure changes with composition from $B8_1$ to the $9R$ at the sulfur-rich end, but the unit-cell volume varies smoothly across this $B8_1$–$9R$ boundary. The $9R$ a and c lattice parameters increase continuously with x as do the $9R$ unit-cell volumes. However, the parameters do not extrapolate precisely to the Ti_8S_9 values reported by Bartram (21). The *a lattice parameters of the* $B8_1$ *samples* found at the selenium-rich end of the compositional scale

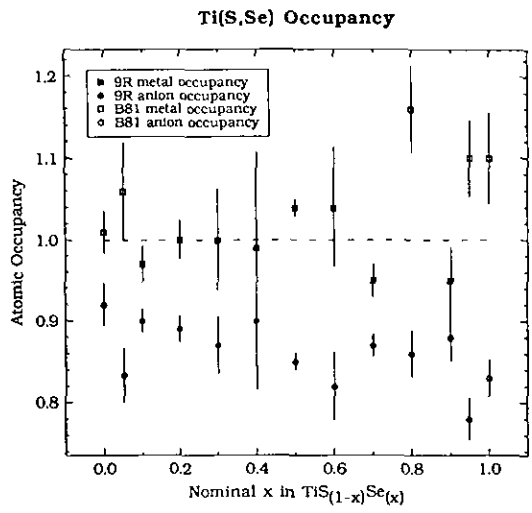

FIG. 6. Atomic occupancies of the $Ti(S_{1-x}Se_x)$ system.

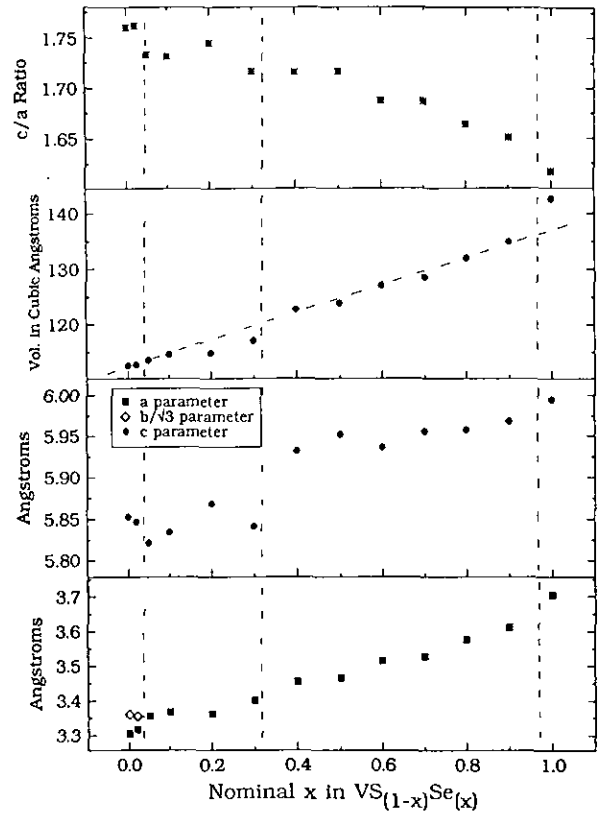

FIG. 7. *Lattice parameters, unit-cell volumes, and c/a ratios for the* nominal $V(S_{1-x}Se_x)$ system.

merge smoothly with the *a* lattice parameters of the *9R* phase, but the $B8_1$ *c* lattice parameters are larger than those of the *9R* phase. This feature is also reflected in the unit cell volumes and *c/a* ratios of the $B8_1$ phase. Extrapolation of the $B8_1$ lattice parameters in the selenium-rich compositions compared to the sulfur-rich compositions suggests a profound difference in the character of these two $B8_1$ phases. Figure 6 and Table 3 illustrate the ratio of Ti to octahedral sites determined from the density measurements. All samples rejected anions during firing. It is noteworthy that the *9R* samples in this system all have a Ti/octahedral-site ratio close to unity, not 8/9 as found in Ti_8S_9. At higher *x* all $B8_1$ samples have a Ti/octahedral-site ratio greater than or equal to 1.1.

The magnetic susceptibilities χ of the $Ti(S_{1-x}Se_x)$ samples exhibit a slightly enhanced Pauli paramagnetism. A contribution from localized spins appears below 10 K. An anomalous dip in the inverse susceptibility occurs between 60 and 70 K in each of the *9R* samples; this anomaly probably reflects a subtle structural change at this temperature in the *9R* phase. All samples were metallic.

TABLE 3
The $TiS_{1-x}Se_x$ System

Nominal composition	(S,Se) : Ti ratio	Density (g/cm³)	Calculated stoichiometry
TiS–$B8_1$	0.93 ± 0.007	4.25 ± 0.012	$Ti_{0.99}S_{0.92}$
$TiS_{0.95}Se_{0.05}$–$B8_1$	0.79 ± 0.032	4.34 ± 0.003	$Ti_{1.06}(S_{0.97}Se_{0.03})_{0.834}$
$TiS_{0.9}Se_{0.1}$	0.93 ± 0.011	4.29 ± 0.006	$Ti_{0.97}(S_{0.94}Se_{0.06})_{0.90}$
$TiS_{0.8}Se_{0.2}$	0.87 ± 0.012	4.46 ± 0.002	$Ti_{1.00}(S_{0.84}Se_{0.16})_{0.89}$
$TiS_{0.7}Se_{0.3}$	0.87 ± 0.031	4.64 ± 0.02	$Ti_{1.00}(S_{0.71}Se_{0.29})_{0.87}$
$TiS_{0.6}Se_{0.4}$	0.91 ± 0.061	4.81 ± 0.02	$Ti_{0.99}(S_{0.63}Se_{0.38})_{0.90}$
$TiS_{0.5}Se_{0.5}$	0.82 ± 0.004	4.93 ± 0.001	$Ti_{1.04}(S_{0.54}Se_{0.46})_{0.85}$
$Ti_8(S_{0.5}Se_{0.5})_9$	0.83 ± 0.040	4.92 ± 0.005	$Ti_{1.02}(S_{0.53}Se_{0.47})_{0.85}$
$TiS_{0.4}Se_{0.6}$	0.78 ± 0.036	5.06 ± 0.007	$Ti_{1.04}(S_{0.39}Se_{0.61})_{0.82}$
$TiS_{0.3}Se_{0.7}$	0.92 ± 0.009	5.15 ± 0.01	$Ti_{0.95}(S_{0.29}Se_{0.71})_{0.87}$
$TiS_{0.2}Se_{0.8}$–$B8_1$	0.75 ± 0.028	5.36 ± 0.008	$Ti_{1.16}(S_{0.32}Se_{0.68})_{0.86}$
$TiS_{0.1}Se_{0.9}$	0.92 ± 0.021	5.48 ± 0.01	$Ti_{0.95}(S_{0.10}Se_{0.90})_{0.88}$
$TiS_{0.05}Se_{0.95}$–$B8_1$	0.71 ± 0.025	5.45 ± 0.01	$Ti_{1.10}(S_{0.05}Se_{0.95})_{0.78}$
$TiSe_{1.05}$–$B8_1$	0.76 ± 0.021	5.74 ± 0.03	$Ti_{1.10}Se_{0.83}$

5.4. The $V(S_{1-x}Se_x)$ System

All prepared samples appeared to be single-phase; however, the X-ray diffraction reflections were quite broad in the range $0.4 \leq x \leq 0.7$, which would indicate considerable chemical inhomogeneity. A high background signal provided evidence of amorphous material. The lattice parameters, unit-cell volumes, and *c/a* ratios of the $V(S_{1-x}Se_x)$ system are displayed in Fig. 7. For $0 \leq x \leq 0.02$, the samples have the orthorhombic $B31$ structure; the remainder of the samples in the series have the hexagonal $B8_1$ structure. The unit-cell volume varies continuously through the $B31$–$B8_1$ transition, but a break occurs in the evolution with *x* of the *c* parameter near $x \cong 0.35$; a first-order expansion is found in the range $0.9 < x < 1.0$. The expansion is in all directions in the crystal, which may signal a change from weakly to strongly correlated itinerant electrons and/or covalent to ionic bonding.

TABLE 4
The $VS_{1-x}Se_x$ System

Nominal composition	(S,Se) : V ratio	Density (g/cm^3)	Calculated stoichiometry
VS	0.96 ± 0.012	4.71 ± 0.006	$V_{0.98}S_{0.94}$
$VS_{0.98}Se_{0.02}$	0.84 ± 0.012	4.61 ± 0.005	$V_{0.97}(S_{0.995}Se_{0.005})_{0.89}$
$VS_{0.9}Se_{0.1}$	0.79 ± 0.026	4.77 ± 0.001	$V_{1.04}(S_{0.93}Se_{0.07})_{0.83}$
$VS_{0.8}Se_{0.2}$	0.74 ± 0.11	5.01 ± 0.005	$V_{1.07}(S_{0.82}Se_{0.18})_{0.80}$
$VS_{0.7}Se_{0.3}$	0.78 ± 0.044	4.95 ± 0.001	$V_{1.02}(S_{0.75}Se_{0.25})_{0.81}$
$VS_{0.6}Se_{0.4}$	0.69 ± 0.033	5.20 ± 0.001	$V_{1.12}(S_{0.61}Se_{0.39})_{0.77}$
$VS_{0.5}Se_{0.5}$	0.63 ± 0.017	5.27 ± 0.002	$V_{1.15}(S_{0.50}Se_{0.50})_{0.72}$
$VS_{0.4}Se_{0.6}$	0.71 ± 0.036	5.37 ± 0.005	$V_{1.10}(S_{0.41}Se_{0.59})_{0.78}$
$VS_{0.3}Se_{0.7}$	0.67 ± 0.012	5.24 ± 0.006	$V_{1.13}(S_{0.34}Se_{0.67})_{0.76}$
$VS_{0.2}Se_{0.8}$	0.68 ± 0.04	5.64 ± 0.01	$V_{1.14}(S_{0.21}Se_{0.79})_{0.78}$
$VS_{0.1}Se_{0.9}$	0.70 ± 0.067	5.82 ± 0.003	$V_{1.15}(S_{0.09}Se_{0.91})_{0.80}$
VSe	0.76 ± 0.015	5.75 ± 0.003	$V_{1.2}Se_{0.84}$

Table 4 shows the calculated stoichiometry for various values of the nominal as-mixed parameter x in the system $V(S_{1-x}Se_x)$ system; the calculations are based on the measured anion/metal ratio and density. The site occupancies, Fig. 8, show once again that the $B8_1$ samples may have interstitial cations may whereas the $B31$ samples do not.

In general, the magnetic susceptibility is small and temperature-independent at the higher temperatures ($T \cong 300$ K). For lower temperatures (in the range 10 to 50 K) evidence of localized moments is also found in this system.

Broadly speaking, the resistances of all the $V(S_{1-x}Se_x)$ samples were low ($R \approx 4 \times 10^{-2}\ \Omega$) and, in the two $B31$ samples, remained temperature-independent to 4 K. However, all the $B8_1$ samples except VSe exhibited an abrupt increase in resistance with decreasing temperature in the interval 75 K $< T <$ 160 K. In an attempt to clarify the origin of this resistive anomaly, electron diffraction was performed at room temperature on crystallites of $V(S_{0.4}Se_{0.6})$. An unusual mosaic structure impeded all efforts to identify the zone axis of the crystal structure; in dark field imaging, finger-like features with a size of the order of 100 Å were observed. The precise nature of this fine-scale microstructure was not determined. Surprisingly the samples remained stable under the electron beam. Small clumps of amorphous material, presumably rejected sulfur and/or selenium, were detected with TEM.

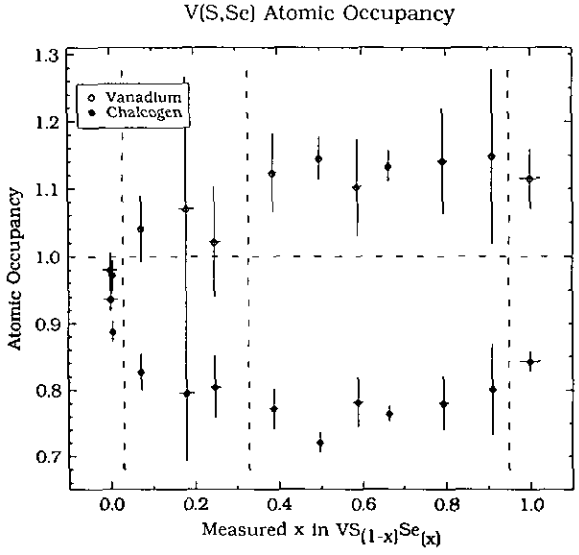

FIG. 8. Atomic occupancies of the $V(S_{1-x}Se_x)$ system.

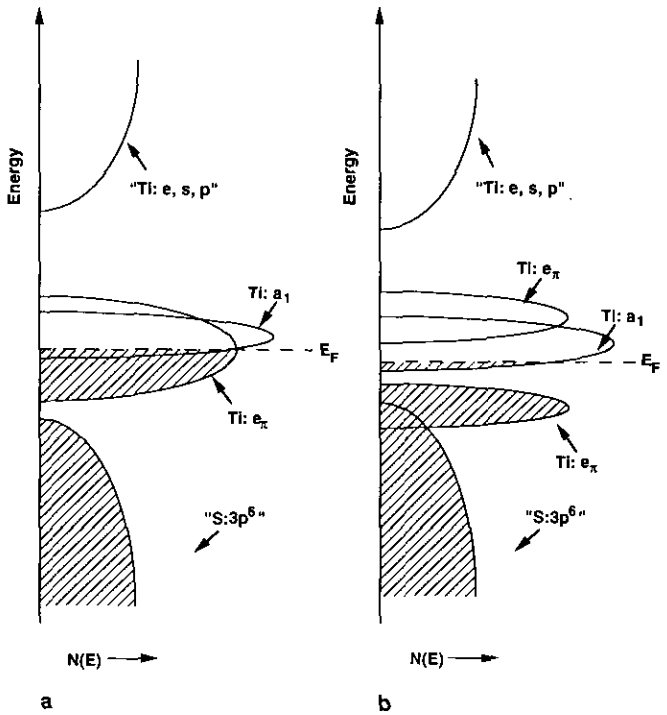

FIG. 9. Schematic energy density of states for outer electrons of (a) $B8_1$ TiS_{1-y} and (b) $B31$ $TiSe_{1-y}$ (anion-vacancy localized states not shown, but added electrons included).

6. DISCUSSION

The band calculations support the following basic features of the valence electrons in TiS, TiSe, VS, and VSe, and their solid solutions: (i) strong metal–chalcogen (M-X) σ-bond interactions create a filled valence band of primarily anion p character and empty antibonding bands of primarily cation s, p, and e orbital parentage; and (ii) the remaining three cation $3d$ orbitals interact less strongly with the anions, but are broadened into narrow $3d$ bands by metal–metal interactions. Two $3d$ bands can be distinguished: an orbitally nondegenerate a_1 band associated with metal–metal bonding along the c-axis across

shared octahedral-site faces and two degenerate e_π bands associated with metal–metal bonding within the basal planes across shared octahedral-site edges.

6.1. *The $Ti(S_{1-x}Se_x)$ System*

A distinctive feature of the hexagonal $B8_1$ structure is the variability of the c/a axial ratio; a large c/a ratio would indicate stabilization of the e_π bands relative to the a_1 band and a small c/a ratio would do the opposite. Moreover, optimum metal–metal bonding occurs where the bands are half-filled. In the case of TiS and TiSe, which have two electrons per Ti atom in the Ti $3d$ bands, stabilization of half-filled e_π bands and an empty a_1 band would maximize bonding in the basal planes without any competition from c-axis metal–metal bonding; this situation favors an anomalously large c/a ratio such as is actually found in TiS. However, the introduction of anion vacancies both adds electrons to the Ti $3d$ bands and allows for shorter M–M distances. The addition of extra $3d$ electrons suggests that the a_1 band is not raised completely above E_F by the large c/a ratio, so we obtain the schematic energy density of states shown in Fig. 9a. Stabilization of phases with a large concentration of anion vacancies is a common feature of binary compounds with metal–metal bonding (49, 50).

In the case of TiSe, the larger size of the anion not only increases the separation between octahedral sites, which narrows the Ti a_1 and e_π bands, but also increases the separation between octahedral and bipyramidal sites sufficiently to allow stabilization of interstitial Ti atoms. Consequently, attempts to prepare stoichiometric, or nearly so, TiSe have yielded four distinguishable phases: (i) a nominal $TiSe_{1.05}$ phase that is hexagonal ($B8_1$ type) with $c/a = 1.764$ (33) and appears to correspond to the $Ti_{1.10}Se_{0.83}$ phase of Tables 2 and 3 with a $c/a = 1.734$; (ii) a cation-deficient phase Ti_8Se_9 with cations that are ordered within alternate basal planes of the $B8_1$ structure and a normalized $c/a = 1.75$ (34); (iii) a rhombohedral phase with a normalized $c/a = 1.69$ (35) recognized in this work to be a $9R$ polytype if 5 mol% of the selenium is substituted by sulfur; and (iv) a nominal $TiSe_{0.95}$ phase that is orthorhombic $B31$ with $c/\langle a\rangle = 1.81$ (33) and appears to correspond, within experimental error, to the $TiSe_{0.87}$ sample of Table 2; $\langle a\rangle = \frac{1}{2}[(b/\sqrt{3}) + a]$ is the mean $B31$ basal-plane lattice parameter.

Distortion of the $TiSe_{1-x}$ phase from the $B8_1$ to the $B31$ structure is accomplished by the formation of two shorter basal-plane M–M bonds on one side of a metal atom at the expense of two longer M–M bonds on the other side. Such a displacive transition is typical of a narrow half-filled band having a negative curvature of the M–M bond potential vs bond length (51, 52). In the case of $TiSe_{1-x}$, each of the two e_π bands would be half-filled, which leads to the observed 60° angle between M–M bonds in the zigzag chains of the $B31$ structure. Moreover, a $c/b > 0.943$ confirms that the driving force for the $B8_1$–$B31$ transition in TiSe is M–M bonding in the basal planes. As shown in Fig. 9b, the distortion opens a gap in the e_π bands at the half-band position. In TiS, the e_π bands are too broad to sustain the distortion.

On the other hand, enhanced M–M bonding may also be achieved by the introduction of interstitial Ti atoms. The shorter separation across a shared site face between octahedral and bipyramidal Ti atoms leads to the formation of a Ti_7 cluster centered at an interstitial Ti atom; these clusters would lower the c/a ratio and stabilize an hexagonal structure as is observed in the metal-rich phase $Ti_{1.10}Se_{0.83}$. Where interstitial atoms are allowed by a larger anion, M–M bondings can also stabilize metal-rich phases. The sulfide ion is not large enough to stabilize interstitial atoms (see Fig. 5), so only anion vacancies are found in the $(V_{1-x}Ti_x)S$ system.

The Ti_8Se_9 phase described by Brunie and Chevreton (34) contains titanium vacancies and therefore has too small an occupancy of the e_π bands for stabilization of the $B31$ structure. In this phase, Ti–Ti bonding along the c axis via a partially filled a_1 band can be expected to compete with Ti–Ti basal plane bonding via electrons in the partially filled e_π bands, and the axial ratio $c/a = 1.75$ is smaller than in TiS.

The $9R$ structure of the $Ti(S,Se)_{1-x}$ system has a filled cation array and anion vacancies which necessitates both c-axis and basal-plane bonding to be present. In fact, the $c/a = 1.69$ found in $TiS_{0.05}Se_{0.95}$ with the $9R$ structure indicates a stronger relative c-axis bonding than in the $B8_1$ type Ti_8Se_9 phase. In the $9R$ structure, the c-axis periodicity introduces a gap in the a_1 band separating a one-third-filled band from the empty a_1 states. An occupancy of two-thirds electron per Ti atom in bonding a_1 states is consistent with the smaller c/a ratio.

6.2. *The $(V_{1-x}Ti_x)S_{1-y}$ System*

Stoichiometric VS and VSe would contain three $3d$ electrons per V atom, which means that the compounds can be expected to have competitive c-axis and basal-plane bonding; the competition must reduce the c/a ratio relative to that found in TiS where, according to Fig. 9a, the basal-plane bonding is near optimal and the occupancy of the a_1 bands is small. Moreover, a larger effective nuclear charge seen by the V $3d$ electrons (analogous to the origin of the lanthanide contraction on moving to heavier rare-earth atoms) reduces the M–M overlap integral for the same M–M separation, so the e_π bands are narrower in VS than in TiS. Consistent with these two predictions is the observed distortion from $B8_1$ to $B31$

symmetry in VS and a smaller $c/\langle a\rangle = 1.73$ compared to 1.92 in hexagonal TiS. Since the $B31$ distortion is stabilized by opening a gap at the half-band position that contains E_F, the e_π bands must be half-filled in orthorhombic VS, which then leaves the a_1 band also half-filled. The schematic energy-density of states for VS should therefore look like Fig. 9b, but with the a_1 band lowered relative to E_F so as to accommodate the extra electrons in a half-filled a_1 band. This picture is consistent with the recent ultraviolet photoemission study of VS by Bensch and Schlögl (53). The introduction of anion vacancies tends to add electrons to the V $3d$ bands; however, the low-temperature susceptibility data indicate that one of the two added electrons per anion vacancy is trapped out by the vacancy.

The substitution of Ti for V in $(V_{1-x}Ti_x)S_{1-y}$ increases the unit-cell volume, but Fig. 1 shows an anomalous deviation from Végard's law and Fig. 2 shows a larger anion-vacancy concentration y in the domain $0.35 \leq x \leq 0.65$ where the competition between stronger like-atom bonding and atomic disorder is greatest. Moreover, it is in this compositional range that there is a discrepancy between the $B31$ structure of arc-melted samples and the $B8_1$ structure of samples reacted at 800°C. Since the atoms do not carry a large effective charge, we suggest that stronger like-atom M–M bonding creates more like-atom clustering in samples annealed at 800°C where the entropic driving force for disordering of the cation is lower. In the range $0 \leq x \leq 0.35$, retention of the $B31$ structure indicates that the e_π bands remain half-filled, so $[x-2(y - y_0)]$ electrons per Ti atom are removed from the a_1 bands, where $y = y_0$ at $x = 0$. Removal of a_1 electrons weakens the c-axis bonding, and the $c/\langle a\rangle$ ratio increases with x; the c/b ratio increases more sharply. The change in $c/\langle a\rangle$ raises the a_1 band relative to the e_π bands, which keeps E_F in the gap of the e_π bands. In the hexagonal ($B8_1$) range $0.65 \leq x \leq 1.0$, the $2(y - y_0) < 0$ contribution adds, rather than subtracts, to the rate of removal of electrons from the a_1 and antibonding states of the e_π bands with increasing x, and the increase in c/a with x is even more marked.

Franzen and Wiegers (28) have followed the evolution with temperature of the lattice parameters of $VS_{1.00}$ through the second-order $B31$–$B8_1$ transition at 630°C. The increase in mean basal-plane parameter $\langle a\rangle$ and decrease in orthorhombicity with increasing T mirror the changes in lattice parameters with increasing x shown in Fig. 1; in both experiments the $B31$ c-axis shows only a mild increase as the orthorhombicity decreases. The arc-melted samples (24) show a continuous decrease in orthorhombicity with increasing Ti concentration to $x = 0.65$; the abrupt change from $B31$ to $B8_1$ in Fig. 1 reinforces the suggestion of metal atom segregation suppressing a long-range cooperative distortion in the range $0.35 \leq x \leq 0.65$ for the samples annealed at 800°C.

6.3. The $V(S_{1-x}Se_x)$ System

Stoichiometric VSe probably cannot be prepared. In our synthesis, nominal VSe is metal-rich $V_{1.12}Se_{0.84}$; it contains interstitial vanadium atoms that stabilize the hexagonal structure with a reduced c/a. The Se/V ratio and interstitial-ion concentration appear to be sensitive to the thermal history of the sample. In the absence of interstitial vandium, a stoichiometric VSe might be expected to have V-3d bands sufficiently narrow to stabilize antiferromagnetic order rather than a distortion to the $B31$ structure. The susceptibility data indicate the presence of long-range magnetic order rather than a distortion to the $B31$ structure. The presence of long-range magnetic order below a $T_N \cong 240$ K and the dilatation of the lattice parameter on passing from nominal $V(Se_{0.9}S_{0.1})$ to nominal VSe (Fig. 7) are consistent with strong electron correlations and vanadium atomic moments. Nevertheless, the addition of interstitial vanadium does complicate any long-range magnetic order below 240 K. Strong electron correlations in the presence of V_7 clusters would account for the higher electrical resistance found in VSe.

The $B31$–$B8_1$ transformation found in the system $V(S_{1-x}Se_x)$ for $0.02 < x < 0.05$ is accompanied by the addition of vanadium to the bipyramidal interstitial sites (Figs. 7 and 8). As noted above, the sulfide array is not large enough to accommodate interstitial V atoms, so stronger V–V bonding is only achieved in VS by a distortion to the $B31$ structure. With the substitution of some Se for S, the anion subarray is expanded and interstitial vanadium can be accommodated in Se-rich clusters. The resulting V_7 clusters stabilize local hexagonal symmetry to suppress the cooperative distortion to the $B31$ structure. Figures 7 and 8 show that a transition occurs from a few to a significant number of interstitial vanadium atoms in the nominal anion range $0.3 < x < 0.4$; the transition is also marked by an abrupt drop in the density of states $N(E_F)$ as determined from the Pauli paramagnetism. Such a change in $N(E_F)$ is to be expected if the formation of metal-anion cluster orbitals lowers spin-paired bonding orbitals below E_F and raises antibonding orbitals above E_F. The very broad X-ray diffraction peaks for nominal $V(S_{0.4}Se_{0.6})$ and the unusual mosaic microstructure observed in this sample with TEM point to a microsegregation into Se-rich and Se-poor regions of about 100 Å size in the nominal anion range $0.3 < x < 0.7$; the vanadium interstitial would be preferentially segregated to the Se-rich domains.

6.4. The $(V_{1-x}Ti_x)Se$ System

Finally the system $(V_{1-x}Ti_x)Se$ shows an abrupt drop in the unit cell volume occurring in the range $0.1 < x <$

0.2; it appears to reflect a loss of the strong electron correlations associated with long-range magnetic ordering in the vanadium-rich selenides. All the hexagonal selenides show evidence of interstitial metal atoms and anion vacancies. The increase in the c/a ratio with increasing Ti concentration x reflects, as in $V_{1-x}Ti_xS$, a decreasing c-axis bonding; a large c/a ratio raises the energy of the a_1 band relative to that of the e_π bands, which reduces the competition between c-axis and basal-plane bonding in favor of bonding in the basal plane. The result is a decrease in the hexagonal lattice parameter a with increasing x despite the larger size of the Ti^{2+} ion.

7. CONCLUSIONS

The nominal systems TiS–VS, TiS–TiSe, VS–VSe, and TiSe–VSe all show properties that are strongly influenced by metal–metal bonding. In TiS, strong Ti–Ti interactions in the basal plane suffer little competitive c-axis bonding, which makes for a large $c/a = 1.92$. Moreover, the basal-plane e_π bands are too broad to stabilize a displacive distortion to the $B31$ structure. However, the larger Se^{-2} ions in TiSe create a larger separation between octahedral sites, and the e_π bands in the basal planes are narrowed. In this case, enhanced Ti–Ti bonding in the basal planes is achieved either by a distortion to the $B31$ phase or by the introduction of Ti atoms into interstitial bipyramidal sites that introduce strong Ti–Ti bonding within Ti_7 clusters. In general, interstitial metal atoms in these systems stabilize an hexagonal structure and form bonding and antibonding cluster orbitals with neighboring octahedral-site metal atoms.

The sulfides do not accept interstitial metal atoms. In VS, the additional d electron introduces competition between c-axis and basal-plane V–V bonding, which prevents realization of as large a c/a ratio as in TiS. Moreover, the e_π bands are narrowed sufficiently to stabilize a narrow-band distortion to the $B31$ structure. In VSe, the e_π bands are narrowed further, which introduces strongly correlated electrons and antiferromagnetism. In this case, distortion to the $B31$ structure is not a competitive alternative, and only a $B8_1$ phase with interstitial vanadium atoms is found even though this "stuffed" phase contains anion vacancies. The introduction of interstitial vanadium creates molecular V_7 clusters within the matrix of strongly correlated electrons.

Anion vacancies are a common feature in these systems; they reduce the unit-cell volume so as to allow shorter M–M separations, but at the expense of adding electrons to the $3d$ bands. In the selenium-rich compounds, anion vacancies are created in the presence of interstitial metal atoms, which demonstrates the stabilization to be achieved by enhanced metal–metal bonding with the interstitial atoms.

Whereas Ti_8Se_9 contains Ti vacancies ordered within alternate basal planes of a close-packed-hexagonal anion array, Ti_8S_9 forms a $9R$ $(chh)_3$ polytype with apparently disordered Ti vacancies. With only 5% substitution of Se by S in $Ti(Se_{1-x}S_x)_{1-y}$, a $9R$ polytype containing essentially no Ti vacancies is stabilized. We suggest this $9R$ polytype may be stabilized by the opening of a gap at E_F in the c-axis a_1 band as a result of the change in c-axis periodicity.

The $(V_{1-x}Ti_x)S_{1-y}$ system exhibits a range of compositions $0.4 \leq x \leq 0.6$ in which the orthorhombic $B31$ phase may be stabilized in arc-melted samples quenched from high temperatures whereas samples annealed at 800°C are hexagonal. In this compositional range, short-range bonding within like-atom clusters appears to compete with entropy to stabilize at lower temperatures a segregation into like-atom microdomains rather than a distortion to the $B31$ structure.

All samples are metallic and Pauli paramagnetic at higher temperatures ($50\ K < T < 300\ K$). VSe appears to stabilize an antiferromagnetic spin-density wave below $T_N = 240$ K that introduces a semiconductor–metal transition at lower temperatures. Other samples uniformly exhibit the presence of some localized-spin paramagnetism at lowest temperatures; we attribute the spins to the trapping of a single electron at an anion vacancy.

A migration of Ti atoms to interstitial sites accompanied by a loss of Se occurs above the $B31$–$B8_1$ transition in nominal $TiSe_{0.95}$, which makes irreversible the displacive $B31$–$B8_1$ transition since interstitial atoms suppress the $B31$ distortion.

On substitution of Se for S, an interstitial-metal component is abruptly stabilized beyond a critical Se concentration. In $V(S_{1-x}Se_x)_{1-y}$, a tendency to segregate into Se-rich and Se-poor regions was deduced, and we suggest there is a high interstitial-metal concentration in the Se-rich microdomains.

ACKNOWLEDGMENT

Financial support from the Robert A. Welch Foundation, Houston, TX is gratefully acknowledged.

REFERENCES

1. J. B. Goodenough, *Prog. Solid State Chem.* **5,** 145 (1971).
2. F. Jellinek, *MTP Int. Rev. Sci.: Inorg. Chem., Ser. One* **5,** 339 (1972).
3. H. F. Franzen, C. Haas, and F. Jellinek, *Phys. Rev. B* **10,** 1248 (1974).
4. R. Huisman, R. DeJonge, C. Haas, and F. Jellinek, *J. Solid State Chem.* **3,** 56 (1971).
5. W. Biltz, P. Ehrlich, and K. Meisel, *Z. Anorg. Allg. Chem.* **234,** 97 (1937).
6. A. Kjekshus and W. B. Pearson, *Prog. Solid State Chem.* **1,** 83 (1964).

7. F. Hulliger, *Struct. Bonding Berlin* **4,** 83 (1968).
8. K. Adachi, S. Ogawa, and H. P. J. Wijn (Eds.) "Pnictides and Chalcogenides," Landolt–Börnstein Tabellen New Series III/27 Subvolume a:
9. F. Jellinek, *Arkiv. Kemi* **20,** 447 (1963).
10. C. N. R. Rao and K. P. R. Pisharody, *Prog. Solid State Chem.* **10**(4), 207 (1974).
11. F. M. A. Carpay, "Philips Research Reports Supplements," 1968.
12. J. Flahaut, *in* "MTP Int. Rev. Sci.: Inorg. Chem., Ser. One" (L. E. J. Roberts, Ed.), Vol. 10. Butterworths, London, 1972.
13. H. F. Franzen, *Prog. Solid State Chem.* **12,** 1 (1978).
14. J. Nakahara, H. F. Franzen, and D. K. Misemer, *J. Chem. Phys.* **76,** 4080 (1982).
15. R. J. Kematick and C. E. Myers, *Inorg. Chem.* **31,** 3568 (1992).
16. J. Silvestre, W. Tremel, and R. Hoffman, *J. Less-Common Met.* **116,** 113 (1986).
17. S. H. Liu, W. B. England, and H. W. Myron, *Solid State Commun.* **14,** 1003 (1974).
18. K. Motizuki, K. Katoh, and A. Yanase, *J. Phys. C: Solid State Phys.* **19,** 495 (1986).
19. K. Motizuki, *J. Magn. Magn. Mater.* **70,** 1 (1987).
20. K. Motizuki and M. Morifuji, *J. Phys. Colloq.* **8,** C8 (1988).
21. S. F. Bartram, "The Crystallography of Some Titanium-Sulfides." Ph.D. Dissertation, Rutgers University, New Brunswick,NJ, 1958.
22. J. Gopalakrishnan, T. Murugesan, M. S. Hegde, and C. N. R. Rao, *J. Phys. C: Solid State Phys.* **12,** 5255 (1979).
23. H. F. Franzen, *J. Inorg. Nucl. Chem.* **28,** 1575 (1966); H. F. Franzen and T. J. Burger, *J. Chem. Phys.* **49,** 2268 (1968).
24. H. F. Franzen, D. H. Leebrick, and F. Laabs, *J. Solid State Chem.* **13,** 307 (1975).
25. A. B. DeVries and F. Jellinek, *Rev. Chim. Miner.* **11,** 624 (1974).
26. I. Tsubokawa, *J. Phys. Soc. Jpn.* **14,** 196 (1959).
27. A. B. DeVries and C. Haas, *J. Phys. Chem. Solids* **34,** 651 (1973).
28. H. F. Franzen and G. A. Wiegers, *Solid State Chem.* **13,** 114 (1975).
29. H. F. Franzen and G. A. Sawatzky, *J. Solid State Chem.* **15,** 229 (1975).
30. E. Hoschek and W. Klemm, *Z. Anorg. Allg. Chem.* **242,** 49 (1939).
31. G. M. Loginov, *Russ. J. Inorg. Chem. Engl. Transl.* **6,** 133 (1961).
32. F. Grønvold, H. Haraldsen, B. Pedersen, and T. Tufte, *Rev. Chim. Miner.* **6,** 215 (1969).
33. F. Grønvold and F. J. Langmyhr, *Acta Chem. Scand.* **15,** 1949 (1961).
34. S. Brunie and M. Chevreton, *C.R. Seances Acad. Sci. Paris* **274,** 278 (1972).
35. H. Hahn and P. Ness, *Z. Anorg. Allg. Chem.* **302,** 2 (1959).
36. H. Hahn and B. Harder, *Z. Anorg. Allg. Chem.* **288,** 242 (1956).
37. T. Hirota, Y. Ueda, and K. Kosuge, *Mater. Res. Bull.* **23,** 1641 (1988).
38. E. Hoschek and W. Klemm, *Z. Anorg. Allg. Chem.* **242,** 49 (1939).
39. E. Røst and L. Gjertsen, *Z. Anorg. Allg. Chem.* **328,** 299 (1964).
40. F. M. A. Carpay, *J. Inorg. Nucl. Chem.* **28,** 2827 (1966).
41. S. Yuri, S. Ohta, S. Anzai, M. Aikawa, and K. Hatakeyama, *J. Magn. Magn. Mater.* **70,** 215 (1987).
42. D. H. Leebrick, M. S. Thesis, Iowa State University, 1974; NTIS, U.S. Dept. of Commerce IS-T-629.
43. L. Henderson Lewis and J. B. Goodenough, *J. Appl. Phys.* **73**(10), 5704 (1993).
44. G. A. Novak and A. A. Colville, *Am. Mineral* **74,** 488 (1989).
45. W. van Gool, *J. Mater. Sci.* **1,** 261 (1966).
46. D. C. Baird, "Experimentation: An Introduction to Measurement Theory and Experiment Design" Chap. 3. Prentice–Hall, Englewood Cliffs, New Jersey 1962.
47. H. F. Franzen and S. Westman, *Acta Chem. Scand.* **17,** 2353 (1963).
48. B. W. Roberts, *Phys. Rev.* **104,** 607 (1956).
49. N. J. Doyle, J. K. Hulm, C. K. Jones, R. C. Miller, and A. Taylor, *Phys. Lett.* **26,** 604 (1968).
50. A. R. Moodenbaugh, Ph.D. Dissertation, University of California, San Diego, 1975.
51. J. B. Goodenough, *Prog. Solid State Chem.* **5,** 145 (1971).
52. J. B. Goodenough, *Ann. Chim. Paris* **7,** 489 (1982).
53. W. Bensch and R. Schlögl, *J. Solid State Chem.* **107,** 43 (1993).